THE ACS SURVEY OF GALACTIC GLOBULAR CLUSTERS. X.
NEW DETERMINATIONS OF CENTERS FOR 65 CLUSTERS

Ryan Goldsbury[1], Harvey B. Richer[1], Jay Anderson[2], Aaron Dotter[2], Ata Sarajedini[3], and Kristin Woodley[1]

[1] Department of Physics and Astronomy, University of British Columbia, Vancouver, BC, Canada;
rgoldsb@astro.ubc.ca, richer@astro.ubc.ca, kwoodley@phas.ubc.ca
[2] Space Telescope Science Institute, Baltimore, MD, USA; jayander@stsci.edu, dotter@stsci.ca
[3] Department of Astronomy, University of Florida, Gainesville, FL, USA; ata@astro.ufl.edu

ABSTRACT

We present new measurements of the centers for 65 Milky Way globular clusters. Centers were determined by fitting ellipses to the density distribution within the inner 2′ of the cluster center, and averaging the centers of these ellipses. The symmetry of clusters was also analyzed by comparing cumulative radial distributions on opposite sides of the cluster across a grid of trial centers. All of the determinations were done with stellar positions derived from a combination of two single-orbit Advanced Camera for Surveys images of the core of the cluster in *F606W* and *F814W*. We find that the ellipse-fitting method provides remarkable accuracy over a wide range of core sizes and density distributions, while the symmetry method is difficult to use on clusters with very large cores or low density. The symmetry method requires a larger field or a very sharply peaked density distribution.

Key words: astrometry – catalogs – globular clusters: general – methods: data analysis

Online-only material: color figures, figure set

1. INTRODUCTION

The need for precise centers of Galactic globular star clusters is more critical today than ever before. For example, there is much work being done searching for intermediate-mass black holes (IMBHs) in globular cluster cores. The masses of these IMBHs are expected to be quite small compared to their galactic counterparts, a few hundred to a few thousand $M_\odot$, and so the distance from the center of the black hole within which the stars would be observably influenced is also quite small. As shown in Anderson & van der Marel (2010), a center that is off by only 12″ can greatly affect conclusions about the presence of an IMBH. Additionally, recent work analyzing the radial distributions of various stellar populations within globular clusters, such as Bellini et al. (2009) and Ferraro et al. (2009), also depends on the precision of the centers used. An incorrect center will dilute the differences between any two radial distributions centered on the same erroneous location.

Historically, coordinates for the centers of globular clusters have been determined by a variety of methods and have been compiled in a catalog made available online by Harris (1996). The parameters in this catalog are still widely used today. The majority of the centers in this catalog come from a list compiled by Djorgovski & Meylan (1993). Of the 143 globular clusters contained in this 1993 list, 109 of the center coordinates come from Shawl & White (1986). The centers from Shawl & White were taken from scanned photographic plates. These scans were smoothed and the center was found with an algorithm known as the SWIRL technique, developed by C.R. Lynds (described in Shawl & White 1980). This method involves analyzing the density over a number of regions symmetrically selected in the *X*- and *Y*-directions, and manually adjusting the center point until the densities in the corresponding X and Y regions are as similar as possible. Uncertainties were given as the standard error of repeated determinations with this method. These center coordinates have stood the test of time quite well, but with the advancement of modern CCDs and better reduction techniques, more precise centers can be determined.

Whereas previous determinations were made on photographic plates and focused on the outskirts of clusters, our measurements here will focus on the central regions. If there are any asymmetries in the stellar distribution, the two methods will not arrive at the same center. The SWIRL method analyzes the symmetry of light from the entire cluster, but has no way to deal with asymmetries in the distribution caused by small numbers of giant stars. We caution that the method discussed here can only be used to determine the center of the star count distribution. The center of mass must be determined through analysis of the dynamics of the cluster.

2. DATA REDUCTION

All of the data used are from the ACS Survey of Galactic Globular Clusters (Sarajedini et al. 2007). A thorough discussion of the reduction methods used for the data can be found in Anderson et al. (2008). A brief summary follows.

Each cluster was observed with the *Hubble Space Telescope*'s Advanced Camera for Surveys (ACS)/WFC for one orbit through each of *F606W* and *F814W*. Each orbit contained one short exposure (to fill in the saturated stars) and four to five deep exposures, which were stepped over the ACS chip gap for more uniform spatial coverage. The catalog was constructed by analyzing the field patch by patch in all the individual exposures simultaneously. In each patch, the brightest stars were found first and fitted with a point-spread function (PSF) that was tailored to each particular exposure, then subtracted to allow fainter neighbors to be found. Only stars that clearly stood out above the known subtraction errors and known PSF artifacts in multiple exposures in both filters were included in the catalog. The very few stars that were saturated even in the short exposures were measured by fitting the PSF to the surrounding unsaturated pixels. The Two Micron All Sky Survey catalog was to used convert the positions measured in the image-based frame into absolute R.A. and decl. The operations that follow in this paper were based on the right ascension and declination coordinates, as well as the *F814W* magnitude
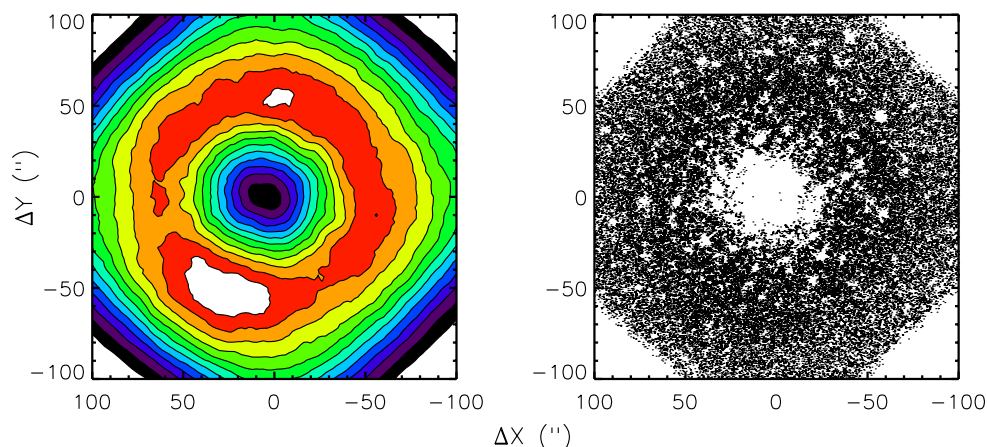
Figure 1. Cluster NGC 1851. The density contours (left) of the stars that were rejected from the center determination method due to the imposed limiting *F814W* magnitude cutoff and positions of the stars in the field (right) after the initial data reduction (star positions are in black). Large voids are seen near brighter stars, as these make it difficult to find fainter stars nearby. The center is almost entirely empty, as it is far too dense to reliably find stars fainter than absolute magnitude 8. The coordinates are in projected distance with respect to the center in the Harris Catalog (1996).

(A color version of this figure is available in the online journal.)

for each star. This entire data catalog will soon be made public.

3. METHODS FOR DETERMINING THE CENTER

Two methods for determining the center of the star count distribution were employed. Both methods begin with the positions and magnitudes from the catalog, constructed as described in Section 2. The density method searches for the average center of a number of isodensity contours by fitting ellipses to these contours. The pie-slice method searches for the most symmetric point of the cluster by analyzing the distributions of stars as a function of radius on opposite sides of the cluster.

All of the centers reported in Table 1 were derived with the density contour method, as it was found to be more reliable over a wide range of density distributions than the pie-slice method. Both of these methods are thoroughly discussed in Anderson & van der Marel (2010), but they will be summarized here as well.

3.1. Density Contours

We began with the catalog as constructed above and converted the apparent *F814W* magnitudes into an absolute magnitude scale using the distance moduli for each cluster from the Harris Catalog (1996). All stars with an absolute *F814W* magnitude fainter than eight were immediately excluded. This has the effect of smoothing out the distribution, as stars fainter than this are not likely to be found near much brighter stars, and they are very incomplete in the cores of denser clusters. When stars of all magnitudes are included in the density distribution, many underdense regions around bright stars appear. These holes do not reflect the true underlying density distribution, and so an arbitrary cutoff was implemented to limit these effects (Figure 1). For denser clusters, stricter magnitude cutoffs were used. The densest clusters required that only stars brighter than an absolute *F814W* magnitude 2 be used, in order to remove the appearance of these holes. These regions of incompleteness begin to significantly overlap as you approach the center of the cluster. The number density of very bright stars in the cores of clusters is so large that very faint stars are almost impossible to reliably detect. As a result, fainter stars are almost entirely incomplete in the inner region of the cluster. Because density

is a function of radius, and the ability to reliably detect a star is dependent on the density of the bright stars in the region surrounding that star, the incompleteness of fainter stars is also a function of radius. So, although incompleteness is also present to a lesser extent in stars above the implemented cutoff, the radial dependence of the incompleteness means that there will be no directional bias introduced by the incompleteness, as evidenced in Figure 2, and center determinations should not be affected.

The coordinate system used for the determination is oriented to right ascension and declination, but with the necessary cosine term to generate a projection onto the plane tangent to the sky at the center of the field. The density of the cluster was then constructed over a grid of points. This grid was centered on the R.A. and decl. from the Harris Catalog (1996). The grid extends $100''$ in each direction, sampling every $2''$. As mentioned in Anderson & van der Marel (2010), significant overbinning is required to generate a smooth distribution. Circular bins were used with a radius of $25''$ in most cases. However, clusters with very flat distributions required larger bins (up to a radius of $40''$) to smooth the distribution. To remove the effects of the edge of the field on the density distribution, the density values for points on the sample grid that were within a bin radius of the edge of the field were set to 0, so as not to be included in any of the contours. That is to say, if the circular bin at that point included area outside of the field, that point was excluded from the ellipse fitting portion of this method.

After the distribution was generated and the edge effects were accounted for, the distribution was broken up into eight contours. The contours were spaced evenly between the minimum non-zero density and the maximum density. The outer three contours were not used due to the fact that they were often quite azimuthally incomplete, and this could potentially bias the ellipse fits. The innermost contour was also ignored as it is actually a solid two-dimensional region of points and could not be fit well with an ellipse. Each of the four remaining contours was then fit with an ellipse. This step is outlined in Figure 3. For most of the denser clusters, it is possible to fit many more than four ellipses (in some cases up to 20). However, larger numbers of smooth contours cannot be generated for the clusters with low numbers and/or flat distributions. In order to maintain consistency, eight contours and four ellipses were adopted as the maximum numbers that could be used for every cluster. The

Table 1
Centers of Milky Way Globular Clusters

| Cluster ID	Alternate ID	R.A. J2000 (h:m:s)	Decl. J2000 (°:′:″)	Estimated Uncertainty (″)	ℓ (°)	b (°)
NGC 104	47 Tuc	00:24:05.71	−72:04:52.7	0.2	282.7334	−29.5475
NGC 288		00:52:45.24	−26:34:57.4	1.8	308.4303	36.0769
NGC 362		01:03:14.26	−70:50:55.6	0.1	316.5174	−12.8101
NGC 1261		03:12:16.21	−55:12:58.4	0.1	316.7442	−60.6231
Palomar 1		03:33:20.04	+79:34:51.8	0.8	133.3390	22.7027
Palomar 2		04:46:05.91	+31:22:53.4	0.1	103.5433	−28.4620
NGC 1851		05:14:06.76	−40:02:47.6	0.1	248.3607	−20.6108
NGC 2298		06:48:59.41	−36:00:19.1	0.1	243.1166	−22.4883
NGC 2808		09:12:03.10	−64:51:48.6	0.1	328.9732	−19.2632
E 3		09:20:57.07	−77:16:54.8	1.5	316.8235	−30.9358
NGC 3201		10:17:36.82	−46:24:44.9	1.0	278.1893	9.2654
NGC 4147		12:10:06.30	+18:32:33.5	0.1	17.7755	65.4396
NGC 4590	M 68	12:39:27.98	−26:44:38.6	0.2	22.8622	−50.2242
NGC 4833		12:59:33.92	−70:52:35.4	0.3	289.7864	−43.0012
NGC 5024	M 53	13:12:55.25	+18:10:05.4	0.1	192.5475	0.2276
NGC 5053		13:16:27.09	+17:42:00.9	1.4	198.6739	11.2637
NGC 5139	ω Cen	13:26:47.28	−47:28:46.1	0.1	273.0120	4.0733
NGC 5272	M 3	13:42:11.62	+28:22:38.2	0.2	43.0822	80.7444
NGC 5286		13:46:26.81	−51:22:27.3	0.1	319.1657	8.1490
NGC 5466		14:05:27.29	+28:32:04.0	0.6	61.6991	6.5728
NGC 5904	M 5	15:18:33.22	+02:04:51.7	0.0	329.0530	62.5516
NGC 5927		15:28:00.69	−50:40:22.9	0.2	330.6481	1.7546
NGC 5986		15:46:03.00	−37:47:11.1	0.2	4.1513	−35.0802
Lyngå 7		16:11:03.65	−55:19:04.0	0.9	274.5328	−55.0366
NGC 6093	M 80	16:17:02.41	−22:58:33.9	0.2	219.5801	−43.8833
NGC 6101		16:25:48.12	−72:12:07.9	0.5	282.8777	−27.5859
NGC 6121	M 4	16:23:35.22	−26:31:32.7	0.4	231.7876	−23.6896
NGC 6144		16:27:13.86	−26:01:24.6	0.6	236.1344	−12.1475
NGC 6171	M 107	16:32:31.86	−13:03:13.6	0.1	233.5681	10.4371
NGC 6205	M 13	16:41:41.24	+36:27:35.5	0.1	186.8649	57.7933
NGC 6218	M 12	16:47:14.18	−01:56:54.7	0.8	272.9232	57.2127
NGC 6254	M 10	16:57:09.05	−04:06:01.1	0.1	339.7755	52.5219
NGC 6304		17:14:32.25	−29:27:43.3	0.2	4.9970	−10.3158
NGC 6341	M 92	17:17:07.39	+43:08:09.4	0.3	74.5945	13.8815
NGC 6352		17:25:29.11	−48:25:19.8	0.6	350.4569	−44.6173
NGC 6362		17:31:54.99	−67:02:54.0	0.5	318.4562	−46.5374
NGC 6366		17:27:44.24	−05:04:47.5	1.4	52.7583	−42.8224
NGC 6388		17:36:17.23	−44:44:07.8	0.3	328.0561	−70.0233
NGC 6397		17:40:42.09	−53:40:27.6	0.3	296.6536	−63.2206
NGC 6441		17:50:13.06	−37:03:05.2	0.2	239.5334	−54.6078
NGC 6496		17:59:03.68	−44:15:57.4	1.3	250.5333	−29.8676
NGC 6535		18:03:50.51	−00:17:51.5	0.4	213.9027	1.2416
NGC 6541		18:08:02.36	−43:42:53.6	0.1	258.8651	−7.1202
NGC 6584		18:18:37.60	−52:12:56.8	0.2	283.3375	5.5601
NGC 6624		18:23:40.51	−30:21:39.7	0.1	288.7654	30.9569
NGC 6637	M 69	18:31:23.10	−32:20:53.1	0.1	317.2313	28.8707
NGC 6652		18:35:45.63	−32:59:26.6	0.1	331.1239	22.9512
NGC 6656	M 22	18:36:23.94	−23:54:17.1	0.8	338.5181	29.5142
NGC 6681	M 70	18:43:12.76	−32:17:31.6	0.1	350.1062	8.1499
NGC 6715	M 54	18:55:03.33	−30:28:47.5	0.1	9.7305	−24.3068
NGC 6717	Pal 9	18:55:06.04	−22:42:05.3	0.2	17.7368	−21.8003
NGC 6723		18:59:33.15	−36:37:56.1	0.3	6.3887	−39.3572
NGC 6752		19:10:52.11	−59:59:04.4	0.1	317.8388	−55.1195
NGC 6779	M 56	19:16:35.57	+30:11:00.5	0.2	127.4063	−32.5365
Terzan 7		19:17:43.92	−34:39:27.8	0.3	260.5393	−79.4448
Arp 2		19:28:44.11	−30:21:20.3	0.9	229.4959	−46.4803
NGC 6809	M 55	19:39:59.71	−30:57:53.1	0.8	241.7989	−11.9084
Terzan 8		19:41:44.41	−33:59:58.1	1.4	247.0191	−8.2681
NGC 6838	M 71	19:53:46.49	+18:46:45.1	0.5	219.2432	55.7621
NGC 6934		20:34:11.37	+07:24:16.1	0.1	51.9165	−18.6097
NGC 6981	M 72	20:53:27.70	−12:32:14.3	0.1	150.5005	−73.7548
NGC 7078	M 15	21:29:58.33	+12:10:01.2	0.2	230.1238	53.5815
NGC 7089	M 2	21:33:27.02	−00:49:23.7	0.1	261.6423	54.6937
NGC 7099	M 30	21:40:22.12	−23:10:47.5	0.1	307.1349	39.5768
Palomar 12		21:46:38.84	−21:15:09.4	0.4	334.1046	34.9822
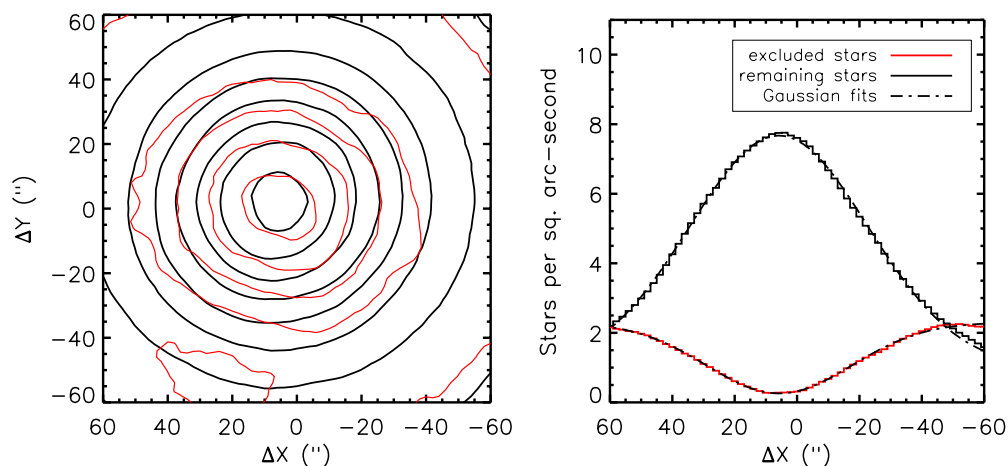
Figure 2. On the left, density contours for NGC 1851 from the method outlined in Section 3.1 are shown in black (thick). Overplotted in red (thin) are the inner contours from the valley shown in Figure 1. Ellipses fit to each of these sets of contours find average centers that agree to within $1\rlap{.}''6$ (within the estimated uncertainty of the two centers). On the right, slices of the density surface are shown through $\Delta Y = 0$ for the faint stars excluded, and the remaining stars used in the center determination. Gaussians fit to these distributions find centers that agree to within $0\rlap{.}''12$. This agreement supports the conclusion that, due to the radial dependence of incompleteness, this effect will not bias the center determinations. The coordinates are in projected distance with respect to the center in the Harris Catalog (1996).

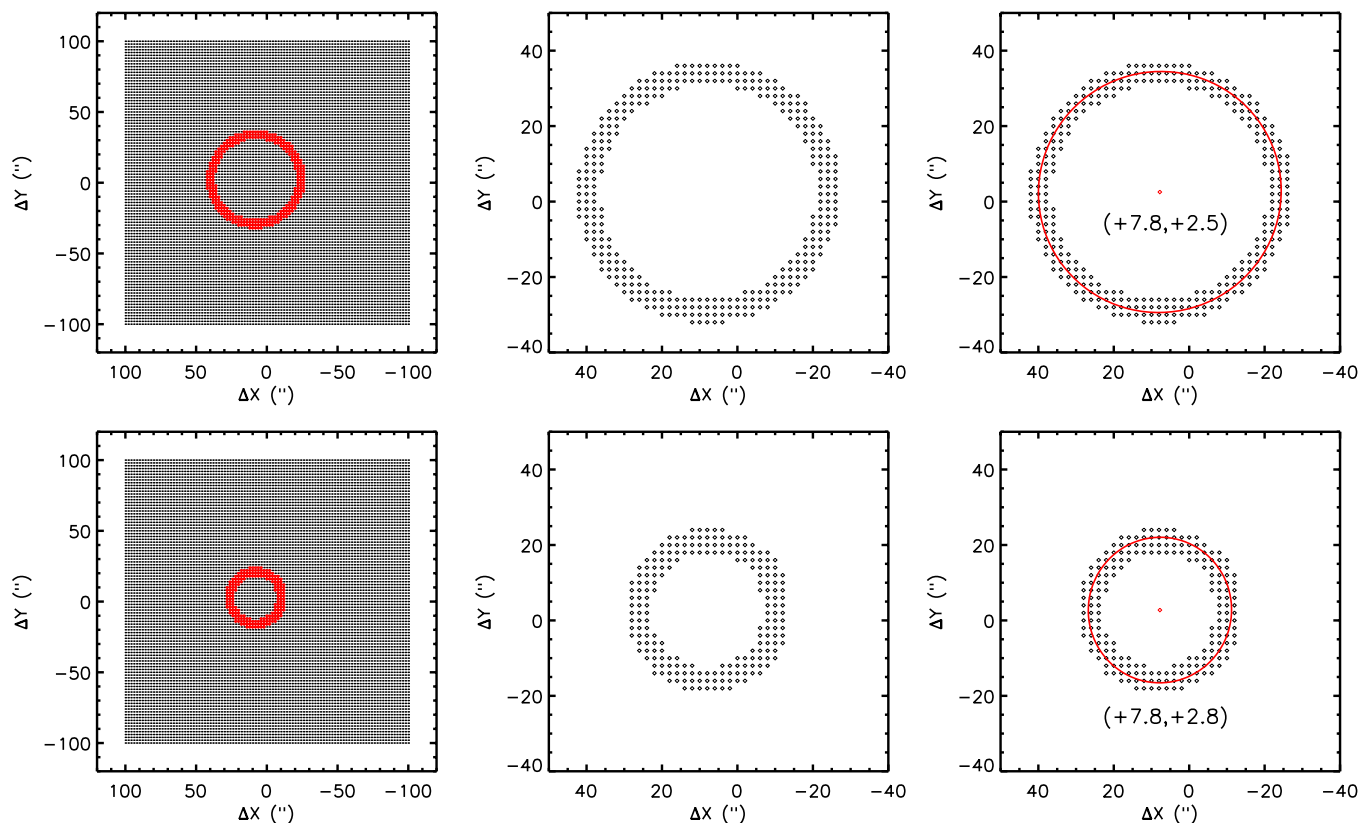(A color version of this figure is available in the online journal.)

Figure 3. Cluster NGC 1851. A visual representation of the method described in Section 3.1. Each row shows the points on the sample grid that fall within a specified density bin, as well as the ellipse fit to these points, and the center for this ellipse. The top row corresponds to a density bin of ∼2.5–3.3 stars per square arcsecond, while the bottom row corresponds to a bin of ∼4.0–4.8 stars per square arcsecond. The coordinates are in projected distance with respect to the center in the catalog (Harris 1996).

(A color version of this figure is available in the online journal.)

final center value was determined as the average center of these four ellipses. The uncertainty was estimated as the standard deviation of the ellipse centers. A plot of the density contours as well as the ellipses fit to these contours and their centers for the cluster NGC 1261 is shown in Figure 4. Plots such as this one are available for all 65 clusters in Table 1 as part of the supplementary material.

The consistency of the method discussed above as well as the error estimates for these measurements were analyzed through bootstrapping. Synthetic cluster distributions were generated and analyzed with the density contours method. The number of stars in the synthetic distributions ranged from 25,000 to 250,000 in increments of 25,000. These values cover roughly the range of the 65 clusters presented in this paper after the
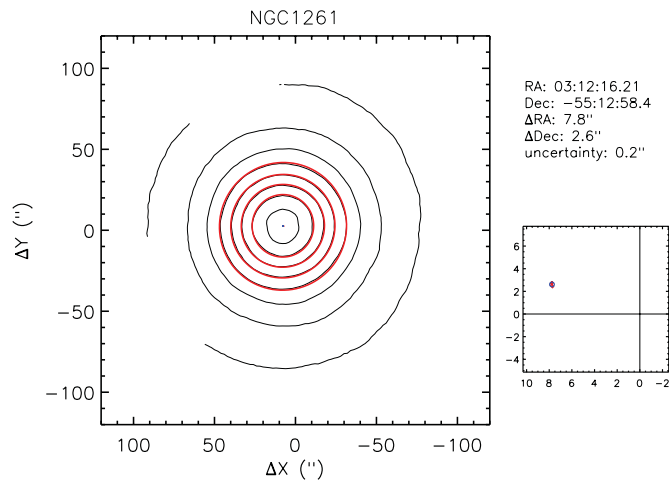
Figure 4. Cluster NGC 1261. Density contours are shown in black (thin). Fit ellipses are shown in red (thick) with the centers as red dots. The calculated center is shown as a blue circle with the radius equal to the estimated uncertainty. Distances are given in seconds of arc in projected distance from the catalog center. Relevant information is contained in the table to the upper right including the center in right ascension and declination, the difference from the catalog center in seconds of arc in the R.A. and decl. directions, and the uncertainty of the center determined as the standard deviation from all of the ellipse centers. The smaller plot in the lower right shows a close-up of the determined center as well as the Harris center, which is [0, 0] in this coordinate system.

(A color version and the complete figure set (65 images) are available in the online journal.)

initial faint magnitude exclusion. For each increment between 25,000 and 250,000, one hundred distributions were generated, and their centers were measured through the density contours method. The standard deviation of the centers used in each determination, as well as the actual errors from the true center of the generated distributions were averaged over these 100 samples. The estimated uncertainty and actual error are plotted against the number of stars in Figure 5. This figure suggests that the standard deviation of the ellipse centers provides a very good estimate of the actual uncertainty in the determination.

A distribution of the differences in X and Y from the catalog centers is shown in Figure 6. X and Y are oriented to R.A. and decl. and represent seconds of arc on the sky. The center coordinates were also compared to those presented in Noyola & Gebhardt (2006). There appears to be no systematic difference between the centers determined in this paper and those determined by Noyola & Gebhardt. The means of the differences in R.A. and decl. are consistent within the standard errors with a distribution about the origin. With respect to the centers in the Harris Catalog, the distribution of differences in X is consistent with a random normal distribution centered around zero, suggesting that there are no systematics biasing the centers in R.A. However, the average difference in the *Y*-direction is greater than the standard error of the differences in that direction, indicating that the distribution is just barely inconsistent with a center of zero. This suggests a possible systematic difference of about $1\rlap{.}''7$ in the decl. direction between the centers provided in Table 1 and the centers given in the Harris Catalog (1996). The centers presented by Noyola & Gebhardt also exhibit this systematic difference with a distribution of differences from the Harris Catalog centered approximately $1''$ south of the origin.

3.2. Pie-slice Contours

To begin, a grid of sample points was constructed around the center value from the Harris Catalog. The grid extends $40''$ in each direction, sampling every $2''$. At each point on the grid, the stars within a radius of $1\rlap{.}''2$ were divided into eight different pie slices corresponding to the cardinal and semi-cardinal directions in R.A. and decl. (see Figure 7). A cumulative radial distribution was then generated for each of the eight pie slices. The four pairs of opposing distributions were then compared. Figure 8 shows two pie slices and the corresponding cumulative distributions of the stars within these regions. To compare the distributions at a single point, the integrated area between the curves was used. Four pairs of distributions were compared, giving four values for each point on the grid. These values were then added together to yield a measure of the symmetry of the cluster at that point on the sample grid. When determined in this way, higher values correspond to less symmetry, as this indicates a
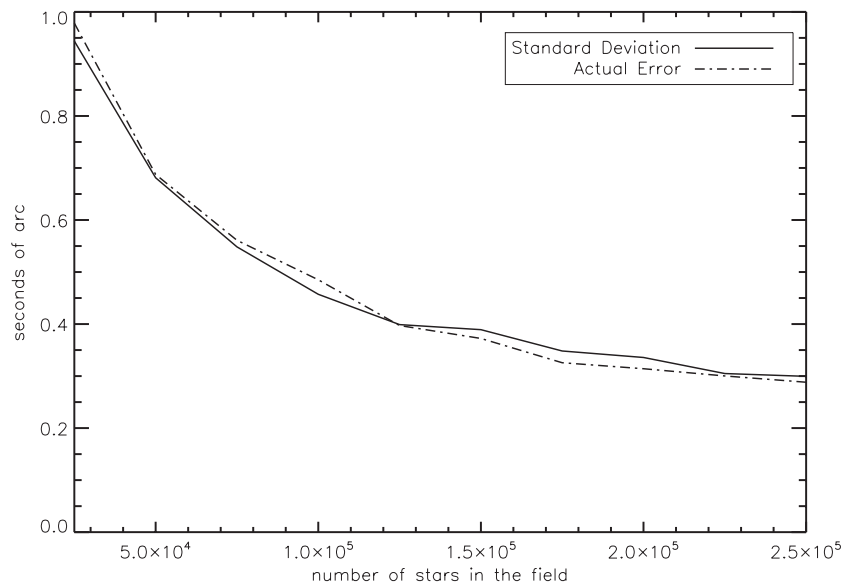

Figure 5. Standard deviation (used as the estimated uncertainty) and actual error as a function of the number of stars in the field. Values were determined through bootstrapping. The standard deviation of the ellipse centers appears to be a good estimate for the uncertainty in the center.
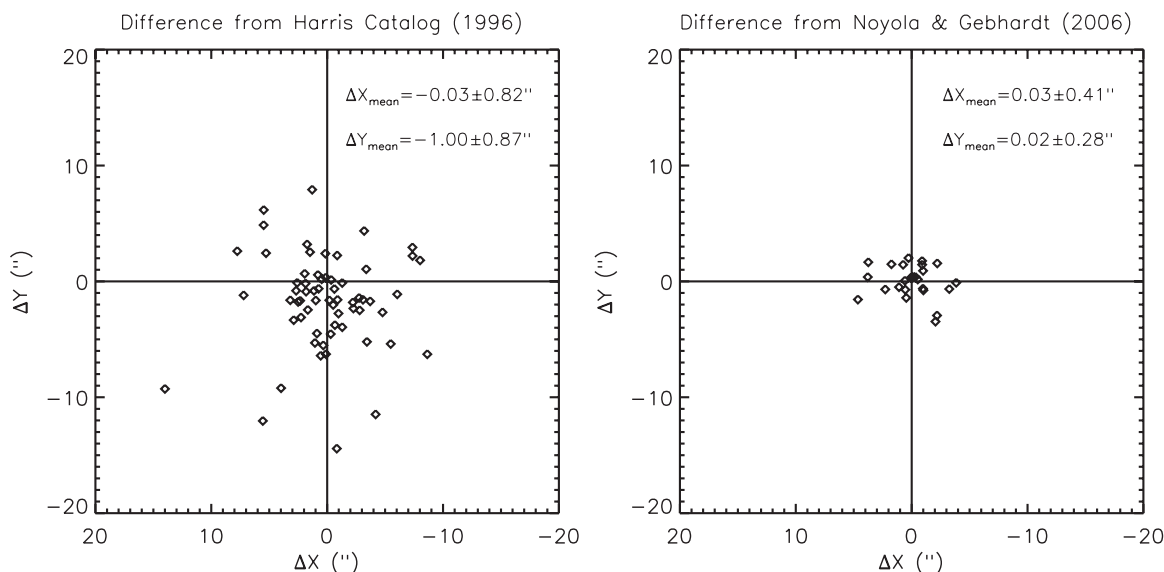
Difference from Harris Catalog (1996)   Difference from Noyola & Gebhardt (2006)

$\Delta X_{mean} = -0.03 \pm 0.82''$

$\Delta Y_{mean} = -1.00 \pm 0.87''$

$\Delta X_{mean} = 0.03 \pm 0.41''$

$\Delta Y_{mean} = 0.02 \pm 0.28''$

Figure 6. Scatter of the differences between the determined centers and the center values given in the Harris Catalog (1996) and Noyola & Gebhardt (2006). The *X*- and *Y*-axes correspond to seconds of arc in the R.A. and decl. directions. The cluster NGC 7089 is not included in the left plot as it differs by greater than 20″; however, it is still included in the average and standard deviation. Cluster NGC 6541 is not included in the comparison to the Harris Catalog at all as our value differs by more than 12′ from the value given there. Of the 65 centers presented in this paper, 24 were also determined by Noyola & Gebhardt (2006). The differences between these 24 clusters are shown on the right. The uncertainties given in each case are the standard error of the mean. With respect to the Harris Catalog, the standard deviation of the scatter in R.A. is 6″65 and the standard deviation of the scatter in decl. is 7″03.
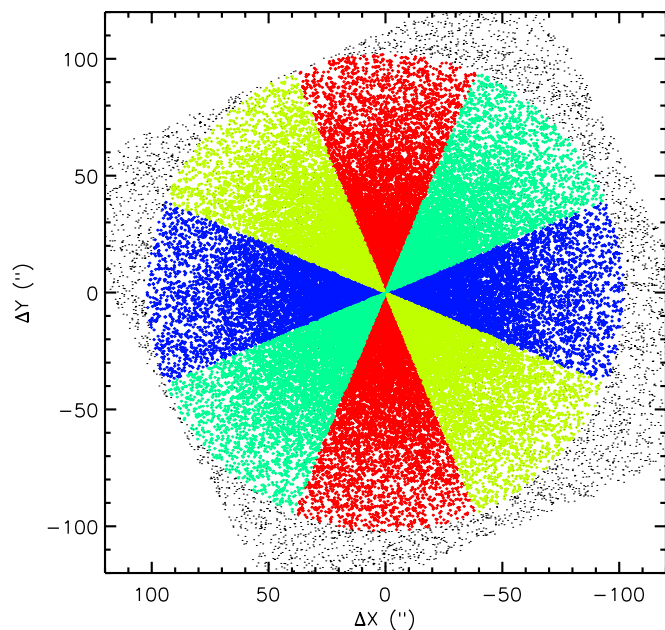
Figure 7. Orientation of the eight pie slices used in the symmetry method are shown here. Each pair is color coded. The cumulative distributions of like colors are compared at each point on a sample grid. The coordinates are in projected distance with respect to the center in the catalog (Harris 1996).

(A color version of this figure is available in the online journal.)

larger difference in the opposing distributions at that point. This was done for every point on the sample grid. The result is a two-dimensional array of values that describe the symmetry of the cluster as a function of position in projected space.

As discussed in the previous section and shown in Figure 1, bright giant stars create large holes in the apparent stellar distribution. These holes are often asymmetrically distributed due to their small numbers, and as a result large differences appear in opposing radial distributions at locations that are otherwise quite symmetric. Because of this effect, many of

the denser clusters required that an incompleteness mask be applied before using the pie-slice method. In this case, simply imposing a strict magnitude cutoff does not work, as this lowers the number of stars in each pie slice to the point where the sample sizes are no longer useful. This is discussed in more detail in Anderson & van der Marel (2010, see Figure 12 of that paper).

It is important to note that a minimum of two pairs of orthogonal pie slices must be used to get a center determination with this method, as each pair of pie slices is only sensitive to changes along one axis. This is demonstrated in Figure 8. Moving a pair of pie slices perpendicular to their orientation keeps them in a position that is still symmetric along their axis. For this reason, a second pair of pie slices must be used to sample the symmetry in the direction orthogonal to the first. For our sample of clusters, it was found that eight pie slices worked better than four; however, switching to 16 pie slices resulted in sample sizes that were too small to be useful.

Determining the size of pie slices to use also takes some consideration. The radius of the pie slices must be determined based on the size of the field and the size of the sample grid. It is important to constrain the radius so that no point on the grid is affected by the edge of the field. It is also important that the radii of the pie slices remain constant across the grid, so as not to bias the determination. This creates a problem, as larger radii create larger samples and thus better distributions, however the sample grid must then be smaller so that the pie slices at the outer edges of the grid do not run out of the field. For this same reason, sampling over a larger area requires the radii of the pie slices to be smaller.

After the symmetry value is calculated at each point in the sample grid, contours can be created and a center determined by finding the most symmetric point on the grid. Due to the orientations of the pie slices, these contours will be eight-sided figures (or 2*N*-sided figures for *N* pairs of pie slices), and so it is not appropriate to fit them with ellipses as discussed in the density contours method. This method can only show the most
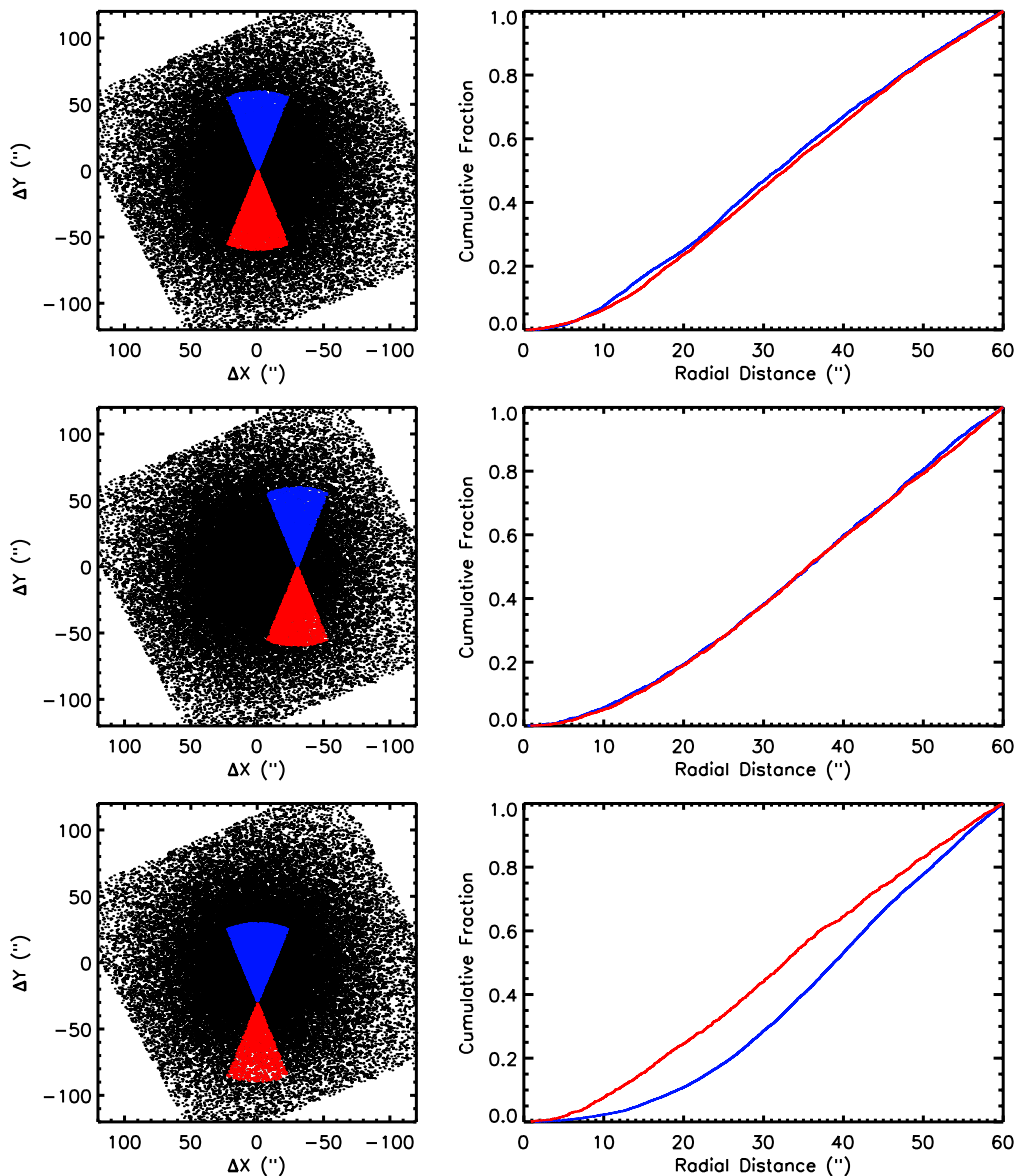
Figure 8. Cluster NGC 1261. The north and south pie slices as well as their cumulative distributions are shown at three different locations in the cluster. The top row corresponds to the center found by the density contours method. The middle row corresponds to a point 30″ west of this center. The bottom row corresponds to a point 30″ south of this center. The distributions remain almost identical as the pie slices are moved perpendicular to their orientation. The area between the opposing radial distributions begins to grow as the pie slices are moved away from the true center of the cluster parallel to their orientation. The coordinates are in projected distance with respect to the center in the catalog (Harris 1996).

(A color version of this figure is available in the online journal.)

symmetric point on the sample grid, and so the uncertainty of this center is limited by the spacing of the grid points. Even for centrally concentrated clusters with good numbers across the field, the symmetry did not appear to change significantly on scales smaller than 2″, and so a grid spacing of less than this was not used. This makes the centers determined by this method considerably less precise than those determined by the density contours method.

4. CONCLUSIONS

In this paper, we have presented new centers for 65 Milky Way globular clusters and outlined the methods used to determine them. All of the centers in are given in Equatorial and Galactic coordinates in Table 1. These centers are significantly more precise than what is currently available in the literature with an average uncertainty of less than 1″. In addition, many of

these centers differ significantly from the values in Harris 1996. Of the 65 clusters analyzed, 26 differ by more than 5″, and 8 clusters differ by more than 10″. Precise centers are key to analyzing the dynamics in the central regions of clusters, and in particular, searching for evidence of IMBHs and analyzing the distributions of separate stellar populations within a cluster. We have described the general outline of the density contours method and shown that incompleteness in faint stars should not bias this determination due to the dependence of incompleteness on the distance from the cluster center. We have also discussed a separate method that relies on analyzing the symmetry of the clusters to find the center, however the dependence of this method on sample size and cluster size relative to the imaging field makes it difficult to apply in most cases. Denser clusters that require masking bright stars can make the symmetry method even more time consuming, and so we suggest that the density

contours method is the preferred method of determing globular cluster centers.

Facilities: HST (ACS)

REFERENCES

Anderson, J., & van der Marel, R. P. 2010, ApJ, 710, 1032
Anderson, J., et al. 2008, AJ, 135, 2055
Bellini, A., Piotto, G., Bedin, L. R., King, I. R., Anderson, J., Milone, A. P., & Momany, Y. 2009, A&A, 507, 1393
Djorgovski, S., & Meylan, G. 1993, in ASP Conf. Ser. 50, Structure and Dynamics of Globular Clusters, ed. S. G. Djorgovski & G. Meylan (San Francisco, CA: ASP), 325
Ferraro, F. R., et al. 2009, Nature, 462, 1028
Harris, W. E. 1996, AJ, 112, 1487
Noyola, E., & Gebhardt, K. 2006, AJ, 132, 447
Sarajedini, A., et al. 2007, AJ, 133, 1658
Shawl, S. J., & White, R. E. 1980, ApJ, 239, L61
Shawl, S. J., & White, R. E. 1986, AJ, 91, 312

ERRATUM: "THE ACS SURVEY OF GALACTIC GLOBULAR CLUSTERS. X. NEW DETERMINATIONS OF CENTERS FOR 65 CLUSTERS" (2010, AJ, 140, 1830)

Ryan Goldsbury[1], Harvey B. Richer[1], Jay Anderson[2], Aaron Dotter[2], Ata Sarajedini[3], and Kristin Woodley[1]
[1] Department of Physics and Astronomy, University of British Columbia, Vancouver, BC, Canada;
rgoldsb@astro.ubc.ca, richer@astro.ubc.ca, kwoodley@phas.ubc.ca
[2] Space Telescope Science Institute, Baltimore, MD, USA; jayander@stsci.edu, dotter@stsci.ca
[3] Department of Astronomy, University of Florida, Gainsville, FL, USA; ata@astro.ufl.edu
Received 2011 May 16; published 2011 July 19

It has come to the attention of the authors that an error was made in calculating the last two columns of Table 1. A coding mistake led to an incorrect conversion of right ascension and declination to Galactic longitude and latitude. A revised table is included below. All aspects of Table 1 aside from the last two columns remain unchanged.

Table 1
Centers of Milky Way Globular Clusters

Cluster ID	Alternate ID	R.A. J2000 (h:m:s)	Decl. J2000 (°:′:″)	Estimated Uncertainty (″)	ℓ (°)	b (°)
NGC 104	47 Tuc	00:24:05.71	−72:04:52.7	0.2	305.8948	−44.8893
NGC 288		00:52:45.24	−26:34:57.4	1.8	151.2815	−89.3804
NGC 362		01:03:14.26	−70:50:55.6	0.1	301.5330	−46.2474
NGC 1261		03:12:16.21	−55:12:58.4	0.1	270.5387	−52.1243
Palomar 1		03:33:20.04	+79:34:51.8	0.8	130.0648	19.0282
Palomar 2		04:46:05.91	+31:22:53.4	0.1	170.5302	−9.0721
NGC 1851		05:14:06.76	−40:02:47.6	0.1	244.5132	−35.0360
NGC 2298		06:48:59.41	−36:00:19.1	0.1	245.6286	−16.0063
NGC 2808		09:12:03.10	−64:51:48.6	0.1	282.1930	−11.2526
E 3		09:20:57.07	−77:16:54.8	1.5	292.2682	−19.0170
NGC 3201		10:17:36.82	−46:24:44.9	1.0	277.2288	8.6404
NGC 4147		12:10:06.30	+18:32:33.5	0.1	252.8485	77.1894
NGC 4590	M 68	12:39:27.98	−26:44:38.6	0.2	299.6257	36.0508
NGC 4833		12:59:33.92	−70:52:35.4	0.3	303.6040	−8.0153
NGC 5024	M 53	13:12:55.25	+18:10:05.4	0.1	332.9624	79.7641
NGC 5053		13:16:27.09	+17:42:00.9	1.4	335.6983	78.9461
NGC 5139	ω Cen	13:26:47.28	−47:28:46.1	0.1	309.1020	14.9683
NGC 5272	M 3	13:42:11.62	+28:22:38.2	0.2	42.2164	78.7069
NGC 5286		13:46:26.81	−51:22:27.3	0.1	311.6142	10.5678
NGC 5466		14:05:27.29	+28:32:04.0	0.6	42.1499	73.5923
NGC 5904	M 5	15:18:33.22	+02:04:51.7	0.0	3.8586	46.7964
NGC 5927		15:28:00.69	−50:40:22.9	0.2	326.6041	4.8598
NGC 5986		15:46:03.00	−37:47:11.1	0.2	337.0221	13.2684
Lyngå 7		16:11:03.65	−55:19:04.0	0.9	328.7690	−2.7973
NGC 6093	M 80	16:17:02.41	−22:58:33.9	0.2	352.6731	19.4631
NGC 6101		16:25:48.12	−72:12:07.9	0.5	317.7461	−15.8248
NGC 6121	M 4	16:23:35.22	−26:31:32.7	0.4	350.9729	15.9722
NGC 6144		16:27:13.86	−26:01:24.6	0.6	351.9288	15.7006
NGC 6171	M 107	16:32:31.86	−13:03:13.6	0.1	3.3732	23.0106
NGC 6205	M 13	16:41:41.24	+36:27:35.5	0.1	59.0073	40.9131
NGC 6218	M 12	16:47:14.18	−01:56:54.7	0.8	15.7151	26.3134
NGC 6254	M 10	16:57:09.05	−04:06:01.1	0.1	15.1370	23.0761
NGC 6304		17:14:32.25	−29:27:43.3	0.2	355.8255	5.3756
NGC 6341	M 92	17:17:07.39	+43:08:09.4	0.3	68.3383	34.8591
NGC 6352		17:25:29.11	−48:25:19.8	0.6	341.4214	−7.1661
NGC 6362		17:31:54.99	−67:02:54.0	0.5	325.5545	−17.5697
NGC 6366		17:27:44.24	−05:04:47.5	1.4	18.4085	16.0357
NGC 6388		17:36:17.23	−44:44:07.8	0.3	345.5564	−6.7377
NGC 6397		17:40:42.09	−53:40:27.6	0.3	338.1650	−11.9595
NGC 6441		17:50:13.06	−37:03:05.2	0.2	353.5322	−5.0057
NGC 6496		17:59:03.68	−44:15:57.4	1.3	348.0269	−10.0137
NGC 6535		18:03:50.51	−00:17:51.5	0.4	27.1755	10.4359
NGC 6541		18:08:02.36	−43:42:53.6	0.1	349.2860	−11.1881
NGC 6584		18:18:37.60	−52:12:56.8	0.2	342.1435	−16.4139
NGC 6624		18:23:40.51	−30:21:39.7	0.1	2.7883	−7.9134

1

Table 1
(Continued)

Cluster ID	Alternate ID	R.A. J2000 (h:m:s)	Decl. J2000 (°:′:″)	Estimated Uncertainty (″)	ℓ (°)	b (°)
NGC 6637	M 69	18:31:23.10	−32:20:53.1	0.1	1.7228	−10.2693
NGC 6652		18:35:45.63	−32:59:26.6	0.1	1.5339	−11.3767
NGC 6656	M 22	18:36:23.94	−23:54:17.1	0.8	9.8922	−7.5516
NGC 6681	M 70	18:43:12.76	−32:17:31.6	0.1	2.8529	−12.5098
NGC 6715	M 54	18:55:03.33	−30:28:47.5	0.1	5.6070	−14.0870
NGC 6717	Pal 9	18:55:06.04	−22:42:05.3	0.2	12.8759	−10.9001
NGC 6723		18:59:33.15	−36:37:56.1	0.3	0.0692	−17.2988
NGC 6752		19:10:52.11	−59:59:04.4	0.1	336.4929	−25.6283
NGC 6779	M 56	19:16:35.57	+30:11:00.5	0.2	62.6593	8.3365
Terzan 7		19:17:43.92	−34:39:27.8	0.3	3.3868	−20.0665
Arp 2		19:28:44.11	−30:21:20.3	0.9	8.5453	−20.7852
NGC 6809	M 55	19:39:59.71	−30:57:53.1	0.8	8.7925	−23.2715
Terzan 8		19:41:44.41	−33:59:58.1	1.4	5.7592	−24.5587
NGC 6838	M 71	19:53:46.49	+18:46:45.1	0.5	56.7458	−4.5643
NGC 6934		20:34:11.37	+07:24:16.1	0.1	52.1032	−18.8928
NGC 6981	M 72	20:53:27.70	−12:32:14.3	0.1	35.1623	−32.6830
NGC 7078	M 15	21:29:58.33	+12:10:01.2	0.2	65.0126	−27.3125
NGC 7089	M 2	21:33:27.02	−00:49:23.7	0.1	53.3708	−35.7696
NGC 7099	M 30	21:40:22.12	−23:10:47.5	0.1	27.1791	−46.8354
Palomar 12		21:46:38.84	−21:15:09.4	0.4	30.5101	−47.6816